SAND2011-7250C 12PFL-1100

Diesel Spray Ignition Detection and Spatial/Temporal Correction

For our reference: Peter M. Lillo, Lyle M. Pickett, Sanghoon Kook, Helena Persson, Öivind Andersson (Do NOT enter this information. It will be pulled from participant tab in MyTechZone)

Affiliation (Do NOT enter this information. It will be pulled from participant tab in MyTechZone)

ABSTRACT

Methods for detection of the spatial position and actual timing of diesel ignition are demonstrated in an optically accessible constant-volume chamber at engine-like pressure and temperature conditions. High-speed pressure measurement using multiple transducers, followed by triangulation correction for the speed of the pressure wave, permits identification of the autoignition spatial location and timing. Simultaneously, high-speed schlieren and broadband chemiluminescence imaging provides validation of the pressure-based triangulation technique. The combined optical imaging and corrected pressure measurement techniques offer improved understanding of diesel ignition phenomenon. Schlieren imaging shows the onset of low-temperature (first-stage) heat release prior to high-temperature (second-stage) ignition. High-temperature ignition is marked by more rapid pressure rise and broadband chemiluminescence. The use of multiple pressure sensors also permits charge-amplifier gain optimization for the needs of the spray, rather than the combustion chamber, thereby providing significantly improved spray pressure-rise measurement and derived heat-release rate. This study provides ignition measurement accuracy with resolution below 20 μs, thereby fulfilling the need for better model validation data.

INTRODUCTION

To meet current emissions regulations and fill the increasing demand for fuel efficiency, diesel engine researchers are working to develop advanced combustion strategies. The increasing variety and complexity of engine combustion strategies, coupled with an improved capability for predictive numerical modeling, has motivated researchers to look towards computational modeling for guidance. Modern spray combustion models typically combine multi-dimensional computational fluid dynamics (CFD) with chemical kinetics for prediction combustion and emissions formation [1-4]. The quality of these numerical models is contingent upon the availability of high-fidelity experimental data for the purpose of validation and improvement [5].

Ignition processes have a strong impact on diesel engine efficiency and exhaust cleanliness [6]. Various parameters affect ignition timing and heat-release rate, including fuel type, injection hardware, injection timing, and cylinder charge conditions. Therefore, a detailed understanding and ability to model these ignition processes is prerequisite to the control and development of advanced diesel engines.

Researchers have established that the basic sequences of ignition include spray air-fuel mixing, fuel vaporization and heat-up, followed by low-temperature (first-stage) heat release and high-temperature (second-stage) ignition (*e.g.*, [6-12]). Based on current modeling capability, however, there is still an incomplete understanding of the progression of ignition, particularly for many fuels and advanced combustion strategies. One level of model fidelity is to faithfully represent the time of ignition. But proper prediction of the spatial location of ignition, as well as the timing, requires much more complete understanding. Typically, the spatial location of ignition is not cross-checked with modeling results, primarily because the spatial location is not known experimentally. Nevertheless, the spatial location of ignition has pronounced effects on combustion and pollutant formation. Recent work has established a connection between the ignition location and the flame lift-off length during the rest of combustion, which strongly affects soot formation within the spray [8,9].

Chemical heat-release events, whether within the low-temperature or high-temperature regime, create propagating pressure waves that are detectible by a sensor. The time delay between the creation of a pressure wave and its registration by a pressure transducer

depends on the gas properties and the distance that lies between. The time lag can be compensated by a speed-of-sound correction, provided that the spatial location of ignition is known. In-chamber acoustics can further complicate pressure signal analysis and obscure relevant heat-release data in noise. Several past publications have focused upon proper handling of pressure and heat-release data acquired in an engine [13-15], but have neglected to focus on the need to make a speed-of-sound correction. Another study cites the existence of the speed-of-sound time lag for pressure data, but reports that filtering for the acoustics waves for in-cylinder pressure data artificially advances ignition timing, thereby partially compensating for the time lag [10].

In most engine research applications, pressure-based diagnostics are the primary source of information concerning heat release and ignition. Rectifying time-lag-induced discrepancies of pressure data acquired from in-cylinder engine testing using a single pressure transducer is usually not possible. For this reason, the application of pressure-based engine data for model validation requires further consideration. Compared to engines with reciprocating pistons, combustion vessels offers a more controlled environment (gas temperature and pressure) that may be preferable for model validation experiments, particularly when equipped with optical access. However, combustion vessels present other difficulties when it comes to pressure and heat-release analysis. Some vessels are continuous-flow, open systems, designed to operate at constant pressure even with combustion. Pressure analysis is possible in constant-volume chambers, but these vessels typically utilize a large chamber volume for gas temperature boundary condition control, resulting in poor signal-to-noise ratio in pressure diagnostics. We will demonstrate how to use multiple pressure transducers to minimize signal-to-noise related issues.

Optical measurements are not limited by speed-of-sound concerns, and various chemiluminescence and laser diagnostics have documented the progression of ignition from a cool-flame (first-stage) combustion to high-temperature (second-stage) ignition and combustion (e.g., [6,7,10]). However, the lack of temporally correlated pressure measurements prohibits a deeper understanding of these optical measurements. A coupling of optical and pressure diagnostics is needed.

Higgins and Siebers coupled optical (chemiluminescence) diagnostics to measured pressure in a constant-volume chamber by applying a speed-of-sound correction to pressure data to report diesel ignition delays [6]. Their method relied on general knowledge of the ignition location based on a series of optical measurements, to calculate the distance from ignition site to the high-speed pressure transducer. Further definition of ignition location, and its impact on heat release derived from pressure was not warranted because of rather coarse data sampling resolution (28 μs). Researchers in all-metal engines have utilized multiple pressure transducers to determine ignition or knock location by triangulation of pressure data [16-18]. Without optical access, the ignition location derived from the triangulation routines is unconfirmed. Simultaneous optical and pressure measurements have been applied to understand knock in spark-ignition engines [19], but no attempts were made determine if knock location could be derived from only the pressure measurement.

In this study we use dual pressure transducers with 5 μs sampling resolution, together with knowledge of the spray penetration direction, to triangulate the ignition location. Simultaneously, we perform dual high-speed chemiluminescence and schlieren imaging to measure the ignition location timing and position directly. Our unique contribution is to use multiple pressure transducers to detect ignition location under diesel-like conditions, and to optically verify the pressure-based triangulation technique. In addition, we present a validation and demonstration on the usage of schlieren imaging for low-temperature heat release. Discussion is also provided on the proper temporal and spatial determination of diesel ignition events.

EXPERIMENTAL APPARATUS AND PROCEDURE

Experiments were performed in a constant-volume combustion vessel at Sandia National Laboratories. The vessel offers a well-characterized gas temperature and pressure environment, spanning diesel-like conditions, making it useful for fundamental spray studies and a source for model validation data. Detail beyond what is provided in this section can be found in references [6-8,20-24].

COMBUSTION VESSEL

The Sandia spray combustion vessel is a pre-burn type vessel designed to generate high in-chamber temperatures and pressures, similar to those of a diesel engine. A premixed charge is spark-ignited and then cooled to the pressure and temperature of interest. A simplified cross-sectional schematic of the combustion vessel is shown in Figure 1.

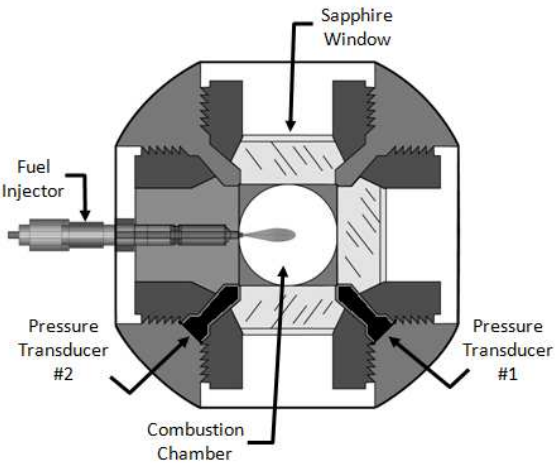

Figure 1: Cross-sectional schematic of the Sandia Spray Combustion Vessel.

The combustion chamber is cubic with six large access ports. For this study, four ports are installed with sapphire windows and two others house the injector and spark plugs. Figure 2 shows a photograph of the vessel. The photograph captures a diesel spray directed towards the viewer, also visible by mirrors at the left and bottom of the vessel. Notice that there are eight corner ports which are typically used for thermocouples, pressure transducers, intake/exhaust valves, and a mixing fan.

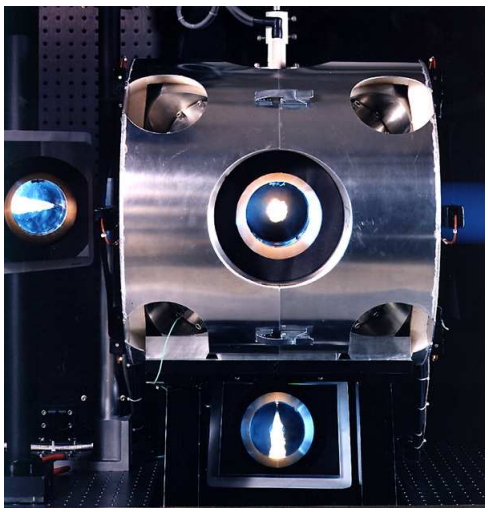

Figure 2: Photograph of the combustion vessel with mirrors showing a flame approaching towards viewer.

Two spark plugs are installed in the top window port of the vessel for pre-burn charge ignition. Much of this study focuses upon the signals acquired from the two pressure transducers which are both labeled in Figure 1. The green wire in the lower left corner of Figure 2 belongs to Pressure Transducer #1. Pressure Transducer #2 is not visible in this photograph, but is installed in the back, lower right corner, opposite the chamber from Transducer #1. As the jet progresses away from the injector tip, its distance to Transducer #1 decreases, and from Transducer #2, increases. Some basic vessel characteristics are given in Table 1, and more detailed chamber dimensions are discussed in the later section on ignition location triangulation.

Table 1: Basic characteristics of combustion vessel

Width of cube	108 mm
Window aperture	100 mm
Chamber volume	1150 cm^3
Injector mounting	Side window
Mixing fan location	Upper corner (opposite

	injector)
Fan speed	1000 rpm
Position of spark plugs	Top window
Body temperature	461 K

For convenience, the test conditions and experimental setup were chosen to be similar to, or the same as, those specified for the Spray A condition by the Engine Combustion Network [20,28]. The high-pressure common-rail fuel injection system is described in Table 2. Additional details on the fuel delivery system and the n-dodecane fuel used can be found in Ref [20].

Table 2: Fuel system properties

Common rail fuel injector	Bosch solenoid-activated, generation 2.4
Injector serial number	210677
Nominal nozzle output diameter	90 μm
Mini-sac volume	0.2 mm^3
Discharge coefficient*	0.86
Spray angle	0° (single axial hole)
Fuel Pressure	150 MPa
Fuel	n-dodecane
Fuel temperature at nozzle	90°C
Actual inject. duration	6.1 ms
Electr. inject. duration	4.45 ms

*using 10 MPa pressure drop and diesel fuel

Premixed fuel/oxidizer charges are prepared external to the combustion vessel. Hydraulically controlled intake and exhaust valves regulate the charge gas intake and exhausting process. A thermocouple installed in one of the corner ports monitors charge gas temperature prior to the pre-burn. The chamber is equipped with in-wall electronic heaters to maintain the prescribed wall temperature, and prevent spent charge condensation.

EXPERIMENTAL PROCEDURE

External to the combustion chamber a premixed gas charge is prepared composed of a combination of oxygen, hydrogen, nitrogen, and acetylene. The composition of the charge is chosen so that, following its complete combustion, the product gas composition is as desired for the start of the spray burn event. The initial reactant mixture may contain excess oxygen such that the product oxygen concentrations are typical of engine conditions (15-21% O_2 concentration). For non-reacting studies, a stoichiometric mixture is used so that the spent pre-burn mixture yields 0% O_2. Density is controlled via charge mass regulation.

At the start of an experiment, the chamber is charged and sealed. A premixed burn is initiated by the spark plugs, increasing both the temperature and pressure of the vessel. The temperature and pressure following the pre-burn are higher than those desired for the experimental spray burn, so the gas charge is allowed to cool via heat transfer to the chamber walls. A mixing fan helps to minimize thermal stratification and promote heat transfer during cool down. Injection is initiated when the in-chamber conditions match those prescribed for the experiment.

The injection duration is 6.1 ms for this study, creating a pressure increase of about 0.15 MPa. The injection duration is short relative to the cool-down time, but long in comparison to a typical diesel spray event. The long injection duration was chosen to allow adequate flame stabilization time over a wide range of test conditions. Figure 3 illustrates a typical pre-burn and injection event pressure history. The pressure increase of the diesel injection event is small in contrast to the peak ambient pressure during the pre-burn.

Following the injection event, the chamber is cooled and vented of the spent charge. A purging process is then initiated, clearing the chamber for the next experiment. Most of the experimental execution is performed electronically by a computer as to increase accuracy, repeatability and safety. Detail about standard combustion vessel operation beyond what is provided in this section can be found in Ref. [20].

PRESSURE MEASUREMENT

The two piezoelectric pressure transducers for this study, referred to as pressure Transducer #1 and #2, are identical (Kistler model K-6001). Each transducer was coupled to a charge amplifier (Kistler model 5010) and sampled at 208 kHz with 12 bit A/D resolution. However, the gain setting of the charge amplifier was different for each transducer as described below.

While a large pressure vessel is convenient for well-controlled (near-uniform temperature and pressure) optical diagnostics, achieving detailed pressure information about a spray event is difficult because it only produces a small pressure rise. The diesel pressure rise is small because of the small mass of fuel injected compared to the large mass of ambient gas within the chamber. One pressure transducer is typically used in this type of facility; with a dynamic range that spans the pressure range of the entire experiment, in this case 0-12 MPa. The large dynamic range of the full-scale sensor, which for our experiments was Transducer #1, comes at the cost of reduced sensitivity and a poor signal-to-noise ratio around the pressure event of interest, the ignition and combustion of the diesel spray.

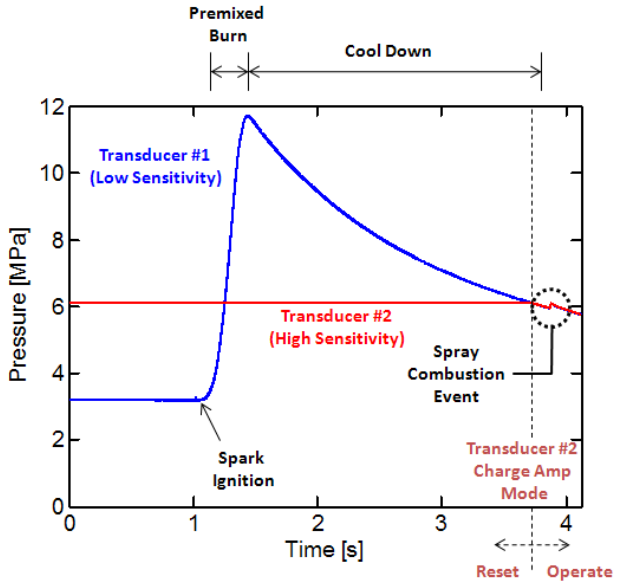

Figure 3: Pressure signals throughout an experiment.

At the loss of total range, the sensitivity of Transducer #2 was increased by setting its charge amplifier to 20 times the gain of Transducer #1. Experiments showed that the system noise was lower by adjustment of the charge amplifier gain compared to applying gain by the analog-to-digital convertor at the computer. With higher sensitivity to pressure, the charge amplifier would saturate and enter overload mode during filling and pre-burn stages prior to the spray event. Therefore, the charge amplifier was kept in reset mode to continuously drain charge from the transducer until just prior to the spray event, as shown in Figure 3.

Figure 3 shows both pressure transducer signals during the pre-burn and the spray event. The high-sensitivity Transducer #2 is placed in “operate” mode at approximately 3.8 s, just prior to the spray event, and it therefore has no useful pressure measurement prior to this time. Meanwhile, the low-sensitivity Transducer #1 operates throughout the charging of the vessel as well as the pre-burn and cool down stages, avoiding saturation throughout the experiment. The low-sensitivity Transducer #1 also provides a needed reference pressure for the high-sensitivity Transducer #2, since the Transducer #2 enters operate mode at a time when the pressure is dynamic and decreasing.

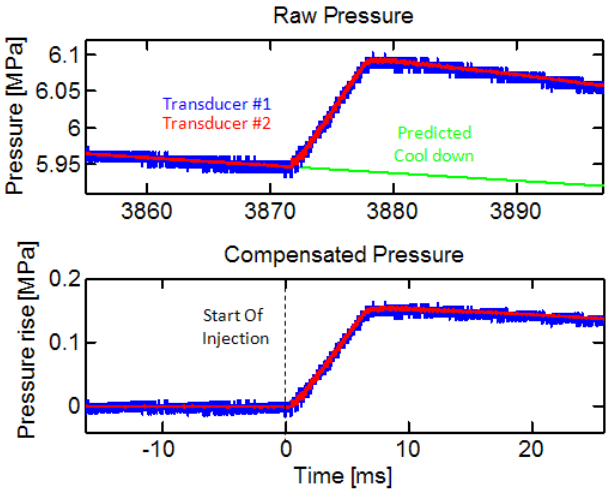

Figure 4: Comparison of pressure signals with and without compensation for heat-transfer and ambient pressure. The time base of the corrected signal has been adjusted relative to the measured start of injection.

During post-analysis, the measured pressure signal is corrected to isolate the spray event. This includes compensation for the rate of charge-to-vessel heat transfer [28]. A comparison between the compensated and uncompensated pressure signals is shown in Figure 4. The fall in pressure prior to injection apparent in the uncompensated pressure signal, is driven by convective heat loss through the chamber walls. The rate of pressure decrease from heat transfer is well characterized by an exponential curve fit, as shown by the green curve at the top of the figure. The compensated pressure rise at the bottom represents the original pressure subtracted by this green curve fit to the pressure decay trend. After this manner, the spray-induced pressure events are separated from the natural vessel pressure decay (heat transfer) prior to injection.

The actual start of injection is detected by monitoring the intensity of a 633 nm HeNe laser which was directed across the tip of the injector. The start of injection measurements were verified through high-speed optical imaging. The compensated pressure signal is adjusted as so that the origin of time reflects the measured start of injection, as can be seen in Figure 4. Since our purpose is to determine actual ignition delay, we will show time after the start of injection (ASI) throughout the paper.

We minimize signal smoothing for the bulk of our pressure analysis to avoid the distortion and loss of information. As discussed in detail by Musculus et al. [3], both the magnitude and duration of premixed burn are dramatically altered by typical pressure smoothing techniques, such as Gaussian low-pass filtering. Higgins and Siebers suggested the usage of a cubic-spline fit for smoothing around the time of ignition, as to best preserve the shape of pressure rise [6]. For the limited pressure smoothing performed in this study, we used a cubic-spline type fit, as will be indicated.

Figure 4 also illustrates the dramatic difference in clarity and noise between Transducer #1 and #2. If space allows, a third pressure transducer could enable high-sensitivity pressure signals at multiple locations. However, as mentioned above, one must use a low-sensitivity transducer in at least one position to provide a reference pressure. In this way, the dynamic range of the system pressure measurement is extended to include fill and pre-burn (low-sensitivity) and spray (high-sensitivity) events.

OPTICAL MEASUREMENTS

Optical techniques were used to visualize ignition and flame progression. Broadband chemiluminescence was imaged at high speed to indicate high-temperature combustion. Simultaneously, high-speed schlieren imaging was acquired to determine the gas-phase jet's progression and timing of ignition. The camera settings for all of the imaging techniques are listed in Table 3 and the setup is shown in Figure 5. The essential elements of these diagnostics have been documented previously [7,22], therefore, only specifics to this study will be discussed.

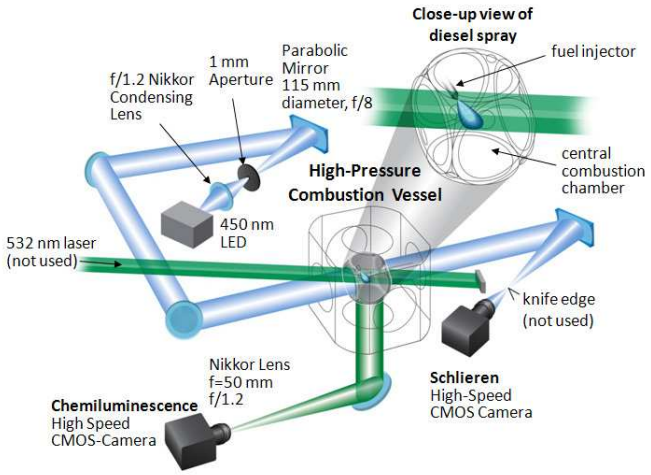

FIGURE 5: Optical setup of high-speed schlieren and chemiluminescence imaging.

Table 3: Camera Properties

	Schlieren	Broadband Chemiluminescence
Camera	Phantom v7.1 CMOS	Phantom v7.1 CMOS
Lens	Nikon 85 mm (f/2.8)	Nikon 50 mm (f/1.2)
Filter	450 nm band pass	600 nm low pass
Framing Period	45.25 µs	50 µs
Exposure	26 µs	46 µs
Resolution	512 x 128	512 x 128

The purpose of the broadband imaging setup was to detect a large range of chemiluminescent species that appear at the onset of high-temperature chemiluminescence, as is described in Refs. [10,26,27]. The 600-nm low-pass filter was used to reject higher wavelength thermal emission from species and later soot incandescence, while permitting collection of other radicals (e.g. CH*, C2*). The broad wavelength collection permitted high-speed operation with a shorter camera gate (46 µs) to temporally resolve the time of high-temperature ignition. Imaging was performed via a mirror at the bottom of the vessel as shown in Figure 5.

Schlieren imaging identifies refractive index gradients within the gas phase. Operating on the principle of sensitivity to refractive index gradients, schlieren imaging is effective in revealing the jet/ambient gas boundaries, as well as gradients that exist within the diesel jet. The setup was a classic Z-type system described in Ref. [25]. Illumination was provided by a 450-nm-centered LED, spatially filtered, collimated with an f/8 mirror, and passed through the combustion chamber. On the other side of the chamber, the beam was re-focused by an f/8 mirror, yielding a focal point approximately 100 mm from the camera collection lens. A schlieren cutoff is typically set at the focal point to enable high-sensitivity to refractive index gradients. However, there is sufficient sensitivity at the conditions of this study (high pressure) such that it is preferable to use no schlieren stop [7,22]. This setup may also be called "focused shadowgraphy" [25]. More detail on this technique can be found in ref [7].

EXPERIMENTAL CONDITIONS

The experimental matrix consists of variables that intentionally change the location of ignition, thereby providing a test of the diagnostics and processing algorithms. Gas temperature has the most pronounced effect on ignition location and lift-off length, therefore, an ambient gas temperature sweep was performed. Three core gas temperatures are highlighted in this paper: 750 K, 900 K and 1200 K. The core gas temperature is defined as the unmixed temperature of the surrounding jet entrainment gases. The relationship between the bulk gas temperature, calculated from the measured pressure, and the core gas temperature was determined via thermocouple measurement [20].

As will be shown, a low ambient gas temperature (750 K) highlights conditions with a long ignition delay and an extended lift-off length [6,8,21]. The intermediate core gas temperature (900 K) is more typical of engine operation and it has been identified as the "Spray A" condition of the Engine Combustion Network (ECN) working group. Extensive data is available for this condition from both Sandia and other laboratories participating in the ECN [20,28]. A core gas temperature of 1200 K produces a very short ignition delays and lift-off length.

The ambient gas composition for this study is given in Table 4. An oxygen mole fraction of 15% corresponds to a diesel engine operating with EGR.

Table 4: Charge and injection gas composition and properties.

	prior to spark ignition [% vol]	**at injection time [% vol]**
O_2 [% vol]	22.63	15.00
N_2 [% vol]	73.82	75.10
CO_2 [% vol]	0	6.20
H_2O [% vol]	0	3.60
H_2 [% vol]	0.50	0
C_2H_2 [% vol]	3.06	0
Average Molecular Weight [g/mol]	N/A	28.96
Ratio of Specific Heats [-]	N/A	1.319
Density [kg/m^3]	22.8	22.8

IGNITION DETECTION TECHNIQUES

Through a combination of schlieren and broadband chemiluminescence imaging and pressure-based techniques, we will characterize diesel ignition with improved spatial and temporal resolution. As previously discussed, there have been many studies focused on diesel ignition phenomenon. Original to this study is a pressure based approach of ignition location triangulation, and the inclusion of schlieren imaging for cool-flame visualization.

TRIANGULATION THEORY

Using multiple pressure transducers and knowledge of chamber geometry, the spatial origin of a heat-release event can be determined. The location of the event then allows a speed-of-sound correction to the time base of pressure to determine the actual ignition delay. This technique has the potential of being algorithmically implemented, and the advantage of not requiring optical access. Even with optical access, the triangulation technique may be useful for detecting ignition location because of the higher sampling rates for pressure data compared to that of imaging systems.

Although the combustion process is inherently three dimensional, the spray penetrates in mainly a straight line in the axial direction. As will be shown, the radial jet displacement due to normal jet spreading does not significantly affect conclusions in this study. Since the spray penetrates in a single direction, a triangulation method to determine the ignition location may be constructed using only two pressure sensors as shown in the diagram in Figure 6.

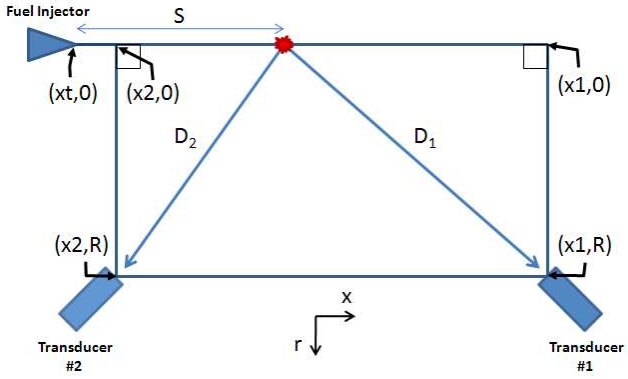

FIGURE 6: Geometry of combustion vessel used for ignition location triangulation.

This view with respect to the axial and radial distances to the pressure transducers is representative of our experimental setup. The relevant dimensions are shown in Table 5.

Table 5: Measured values of experimental setup dimensions shown in Figure 6.

Dimension Label	Dimension Measurement [mm]
R	57.4
x1	94.0
x2	13.7
xt	14.4

We now discuss the algorithm to determine the ignition location and time correction to determine ignition. A pressure wave traveling at a speed of c through a distance D, will take a time t to reach a location through the basic proportional relationship.

$$t = \frac{D}{c} \qquad (1)$$

For any given heat-release event, the delay that each pressure transducer experiences in registering the event is unique. The difference in delay time between pressure transducer signals, which we will refer to as dt, may be obtained by mutual recognition of a single physical heat-release event. Through the combination of dt, an estimated speed of sound c based on the ambient temperature, and knowledge of the transducer location, the heat-release event location is determined with respect to space and time.

The time delay between pressure sensor positions is expressed as:

$$dt = t_2 - t_1 = \frac{D_2}{c_2} - \frac{D_1}{c_1} \qquad (2)$$

And then assuming $c_2 = c_1 = c$,

$$dt = \frac{[(s+xt-x2)^2+R^2]^{1/2}-[(x1-s-xt)^2+R^2]^{1/2}}{c} \qquad (3)$$

Through the measurement of dt, and determination of an average speed of sound, c, the location of a heat release event is determined. This location will be expressed as the axial distance beyond the fuel injector tip, or s, throughout this paper.

SPEED OF SOUND DETERMINATION

The speed of sound in an ideal gas is given by the equation

$$c = \sqrt{\frac{\gamma RT}{M}} \qquad (4)$$

Where γ is the ratio of specific heats, R is the universal gas constant, T is temperature [K], and M is molecular weight. The average molecular weight and γ of the of the 15%-O_2 charge gas are listed in Table 4. The effects of fuel mixed with the ambient on the speed of sound are not considered here because the jet is constrained to a fairly narrow radial distance, as mentioned previously. The correction is primarily dictated by the state of the ambient gases.

The temperature distribution between the ignition site and the transducers must be known to apply the above equations. Non-uniformities will cause uncertainties in the gas speed of sound, and the spatial and temporal correction. Previous studies in the same combustion vessel quantified the thermal stratification [20], showing that there is negligible change along the axis of the jet, which is in a horizontal plane, but buoyancy forces lead to stratification in the vertical direction of approximately 5% for every 15 mm below the jet. As the transducers are positioned lower than the spray, we account for these temperature differences to estimate the speed of sound. Based on extrapolation of the measured gas temperature distribution, we estimate a 15% lower temperature at the pressure transducers. Because temperature is not linearly related to the speed of sound, the following relation is used to determine an effective temperature, which is subsequently used in Eq. (4) to determine the speed of sound.

$$T_{eff} = \frac{(\sqrt{T_{core}}+\sqrt{T_{transducer}})^2}{4} \qquad (5)$$

Although the variation in temperature between the ignition site and the spray causes some uncertainty, this uncertainty ultimately has negligible effects on the applied correction. Figure 7 demonstrates the temperature dependence of the triangulated heat-release axial distance relative to the injector according to Eqs. (3)-(4). The figure shows that even a 500 K difference in gas temperature causes less than a 10 mm change in heat-release location for worst-case positions of 10 or 80 mm. At an axial distance of 10 mm, a variance in 50 K of the estimated T_{eff}, well within experimental uncertainty, yields only a 0.7 mm variance in predicted heat-release location. At 35 mm, the induced spatial error becomes negligible (<0.1 mm). Therefore, even without a complete understanding of the thermal stratification within the vessel, the error induced by this approximation is minimal. As such, potential variances between c_1 and c_2 are neglected because of the minimal sensitivity to ambient gas temperature.

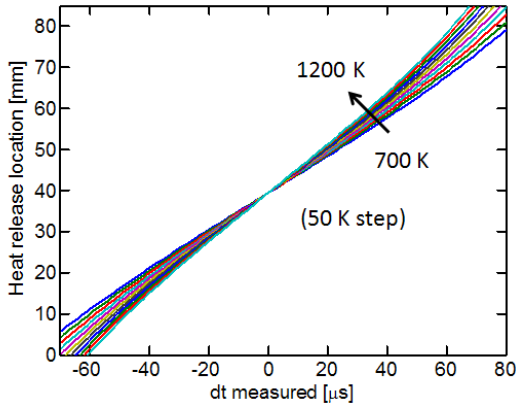

Figure 7: Temperature and dt dependence of flame location measurement.

In practice, the correction technique discussed above is applied only during the time of ignition, a time when the *dt* determination between pressure sensors can be measured accurately. Once reaction begins, heat release occurs over a larger volume of the jet, and temperature and composition varies in the product gases, making it more difficult to derive the origination of multiple heat-release sources.

TIME CORRECTION OF PRESSURE SIGNAL

With knowledge of the heat-release location and the effective speed of sound, the time base of the pressure signal can be corrected to correspond to the actual heat-release timing, rather than the time that the pressure wave reaches the sensor.

Figure 8 shows how this time delay varies with both flame location and effective temperature for the two pressure transducers. The plotted quantities are the variables t_2 or t_1 as solved by Eqs. 2-5 for different values of s. Depending upon the flame location relative to the sensor, different time corrections are applied. The time correction approaches 200 μs, which would have significant implications on diesel ignition understanding and modeling. Notice that the magnitude of the pressure delay is always greater than 80 μs because of the radial offset to the transducers.

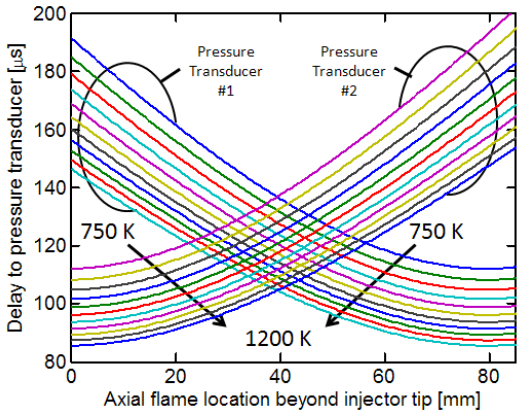

Figure 8: Dependence of measured pressure event delay time on temperature and flame location.

DETERMINATION OF TIME DELAY (*dt*) BETWEEN SENSORS

Analysis of each pressure measurement permitted determination of the time delay of heat-release information to each sensor. Although the ultimate goal is an automated algorithm to find *dt*, we found that results were more accurate with manual processing for the range of data considered in this paper. For detection of *dt*, the raw pressure data is used, rather than averaged or smoothed data. Single-injection analysis is emphasized to test the robustness of the method and to obtain statistics about ignition events that may be highly stochastic. The first recognizable combustion event is manually identified on the two raw pressure signals, and *dt* is determined by shifting the two signals in time with respect to each other. With *dt* known, the heat-release location and relative pressure delay to each transducer follow, as discussed above. Then the calculated delay may be subtracted from the time base for each of the two pressure transducers, placing the start of combustion in its proper experimental time.

The most signature pressure-rise event is the first occurrence of high-temperature heat release leading into the pre-mixed diesel burn. The fraction of pre-mixed burn to mixing-controlled burn, as well as the extent of low-temperature heat release varied between the low- and high-temperature conditions. Therefore, recognizing a signature of the start of combustion is different for each condition.

The manual alignment technique used to determine *dt* is shown in Figures 9, 10 and 11 for the three different ambient gas temperatures. For all examples, the difficulties and limitations of the less-sensitive Transducer #1 signal are recognizable. The raw signal of Transducer #1 falls within the A/D bit resolution (5 kPa) prior to injection, and the digitization appears to be swapping bits. Accurate detection of ignition requires the pressure rise from heat release to rise above this noise floor. Meanwhile, with higher charge amplifier gain, Transducer #2 shows much lower noise prior to ignition, with a strong discernable signal corresponding to ignition events.

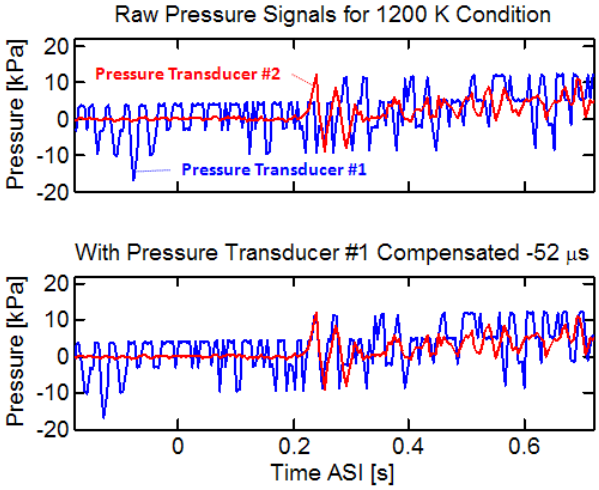

Figure 9: Alignment of two pressure signals to determine dt for the 1200 K condition, test #3.

Figure 9 shows the alignment of two pressure signals for a single injection at 1200 K, the highest ambient temperature for this study. A shift in time of 52 μs aligns the two signals nicely with a strong heat-release event occurring shortly after 0.2 ms. Prior to this time, the pressure signal shows no measureable low-temperature heat release (increase in pressure) or charge-cooling (decrease in pressure)—the trace is essentially flat. After ignition, strong acoustic waves begin. Pressure rise even falls below zero momentarily, but then gradually increases with increasing time after injection as the spray develops. The strong initial heat release shows excellent coherence in the two pressure signals, making determination of *dt* fairly straightforward. But afterwards, the two signals appear to deviate from each other towards incoherency. The lack of coherency in *dt* after ignition is expected, as the combustion region expands to different spatial locations and the reacting sections of the jet progress to a quasi-steady state location. Heat release from many different spatial locations contributes to raise the pressure of the combustion chamber.

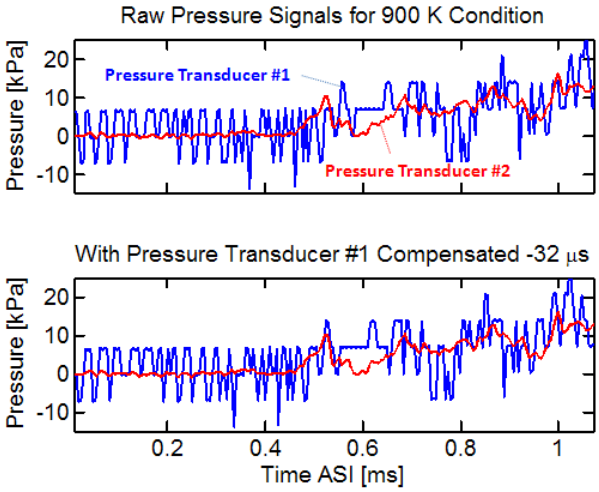

Figure 10: Alignment of two pressure signals to determine dt for the 900 K condition, test #3.

Figure 10 shows the pressure trace alignments for the 900 K test condition. The first combustion event is not as violent, producing a weaker signature than that of the 1200 K condition, but it is still recognizable. A 32 μs time shift provides good coherency between the two measured pressure signals shortly after 0.5 ms ASI, with acoustic oscillations visible after this time.

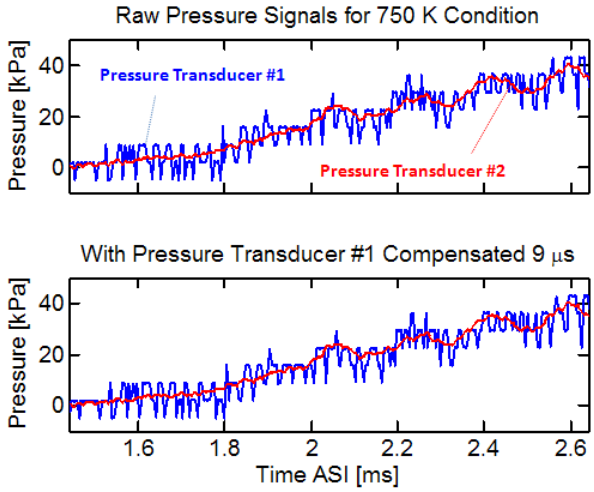

Figure 11: Alignment of two pressure signals to determine dt for the 750 K condition, test #3.

Figure 11 shows that the pressure trace is different for the 750 K condition, compared to either 1200 K or 900 K. There is a weak, gradual rise in signal prior to the start of stronger pressure oscillations. The oscillations are more difficult to detect than at other conditions, but a distinct rise and oscillation begins at approximately 2 ms, indicating rapid heat release. The peak near 2 ms is chosen for time alignment between the pressure traces, and the *dt* is quite small, only 9 μs. The pressure rise beforehand is more gradual and it originates partly from low-temperature combustion. Although the rate of pressure rise is slower, the total heat release is substantial.

Pressure increases almost 5 kPa during the time period between 1.4 to 1.8 ms (preceding ignition), compared to very little pressure rise prior to ignition at 1200 K or 900 K conditions. A contributing factor is that, as the ignition delay is long, a large amount of fuel and ambient gases are already mixed and can participate in low-temperature combustion to produce more cumulative heat release.

Although *dt* is found for all conditions with confidence through this manual alignment technique, implementation of an automated algorithm to recognize the small pressure events would be difficult without improved signal quality. As mentioned above, a third pressure transducer with high-sensitivity could be utilized for this purpose.

Table 6 shows the determined *dt* values for nine different injections, three at each temperature. These specific injections were chosen at random as examples of the triangulation routine capability, but the results are consistent for the entire dataset analyzed, including other ambient temperatures.

IGNITION TRIANGULATION RESULTS

With the measurement of *dt* for each condition, the ignition location is determined using other quantities for the ambient gas listed in Table 6. The ignition location, as well as the time delay to each pressure sensor, are indicated for nine example experiments.

Table 6: Temperature, speed of sound, ignition location, and transducer time delay results.

Test Condition	Core T T_{core} [K]	Eff. T (Eq. 5) T_{eff} [K]	Sound speed c [m/s]	$t_2 - t_1$ dt [μs]	Ignition location s [mm]	Trans. #1 delay t_1 [μs]	Trans. #2 delay t_2 [μs]
1200K (#1)	1206	1114	646	-45	12.8	136	91
1200K (#2)	1202	1110	645	-50	9.6	140	90
1200K (#3)	1207	1115	646	-52	8.1	142	90
900K (#1)	908	838	561	-28	25.6	141	113
900K (#2)	909	839	561	-28	25.6	141	113
900K (#3)	906	836	560	-32	23.5	143	111
750K (#1)	751	694	510	26	51.1	126	152
750K (#2)	752	695	510	27	51.6	125	152
750K (#3)	754	696	511	9	43.5	133	142

Notice that the calculated delay for the ignition pressure wave to reach the transducers is between 90 to 152 μs corresponding to the *dt* of 9 to 52 μs. These time delays indicate that a substantial time correction is needed to understand the actual timing of ignition. Moreover, the time correction is different for each sensor, as it depends upon the distance between the ignition event and that particular sensor.

The ignition results are consistent with expected trends for developing jets, both spatially and temporally. When ignition delay is short, the ignition location occurs near the injector, as mandated by the short axial penetration of the jet very early after the start of injection. We will now evaluate the accuracy of the pressure-sensing technique by direct measurement and comparison of the spatial location and timing of ignition using optical techniques.

SCHLIEREN/LUMINOSITY IGNITION IMAGING

Sequences of images focused around the time of ignition are shown for each of the three experimental conditions in Figures 12, 13 and 14. These figures feature schlieren images overlaid with the high-temperature reaction borders. Refractive index gradients originating from two different sources are apparent in the schlieren images: (1) the vaporizing spray and (2) temperature non-uniformities of gases along the boundary layer of the vessel windows [7,20]. Unfortunately, the overlap of the two makes it difficult to clearly discern the jet. As discussed in Ref. [7], a helpful visualization tool is to plot the difference of subsequent images ($I_n - I_{n-1}$) in the high-speed sequence. We show the $I_n - I_{n-1}$ image at the top of the image sequence, followed by raw schlieren images. Since changes in the jet position are fast compared to that of the slow-moving gases along the walls of the chamber, the envelope of the jet becomes apparent. Careful examination of the change in texture in the raw schlieren images also reveals the border of the jet, which is perhaps most easily visualized at the head of the jet. The raw schlieren images are shown for the majority of the time sequence to illustrate effects of heat release on the schlieren effect, and to also provide a reference for the position of the penetrating jet.

The blue boundaries indicating high-temperature combustion are obtained via post-processing for detection of the first measureable broadband chemiluminescence from a second high-speed camera. A luminosity intensity threshold is chosen at 5% of the camera full range, far enough above the noise floor of the camera, to indicate the first measureable luminosity. Recall that the schlieren and chemiluminescence cameras are orthogonal to each other (Figure 5), so that information is primarily comparable only along the axial direction, rather than radial direction. As both schlieren and chemiluminescence imaging are line-of-sight diagnostics, heat release might be occurring anywhere along the radial path through the jet. Although images were obtained simultaneously during the same injection, note that the framing rate and exposure duration for the broadband chemiluminescence and schlieren cameras are not the same. The schlieren image sequence has tighter temporal resolution. With a chemiluminescence framing period of 50 μs, the temporal offset between schlieren and chemiluminescence images may be as large as 25 μs on some of the overlaid images. The time of the schlieren image is displayed in pink, and the time of the chemiluminescence in blue. Each image time-stamp is associated with the actual exposure timing, for which we have chosen the time halfway through the exposure to be representative. High-speed image data are aligned with the pressure data and actual start of injection, by recording the camera trigger and HeNe laser transmission past the front of the injector with computer data acquisition.

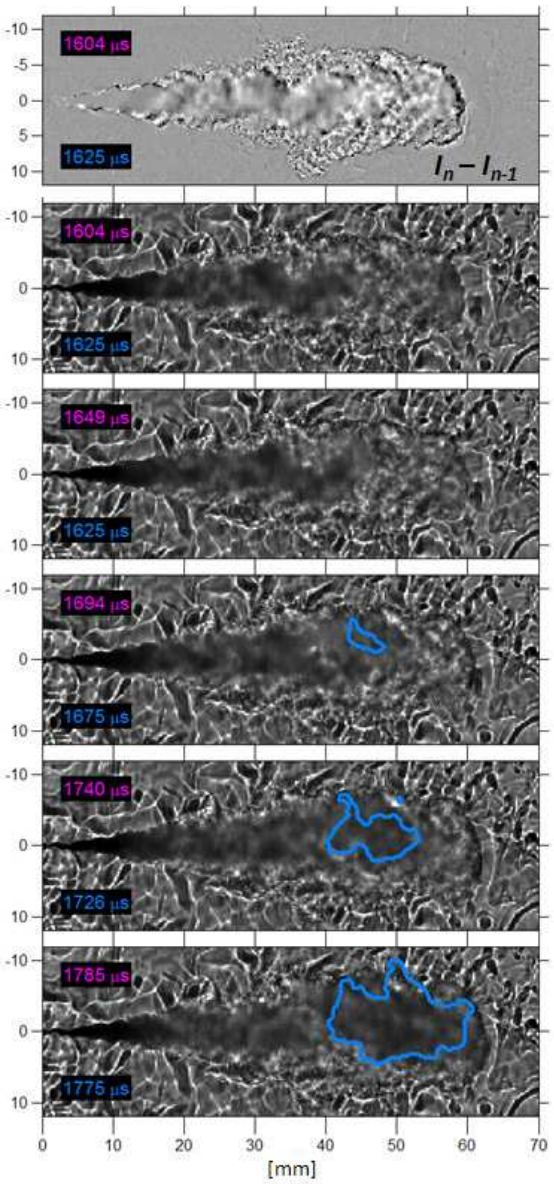

Figure 12: Schlieren images overlaid with broadband luminosity borders (blue) for the 750 K condition, test #3.

At the time of first high-temperature chemiluminescence for the 750-K condition, 1675 μs, the jet has penetrated approximately 55 mm. The first ignition site appears slightly upstream of the penetrating head of the fuel jet at approximately 45 mm. With a careful

eye, one can see that in the first two frames, prior to ignition, the downstream jet edges and ignition zone lighten, or the schlieren effect appears more transparent. Upon the onset of high-temperature heat release, the reaction zone darkens, as can be seen in the last two frames. These effects will be discussed in detail later.

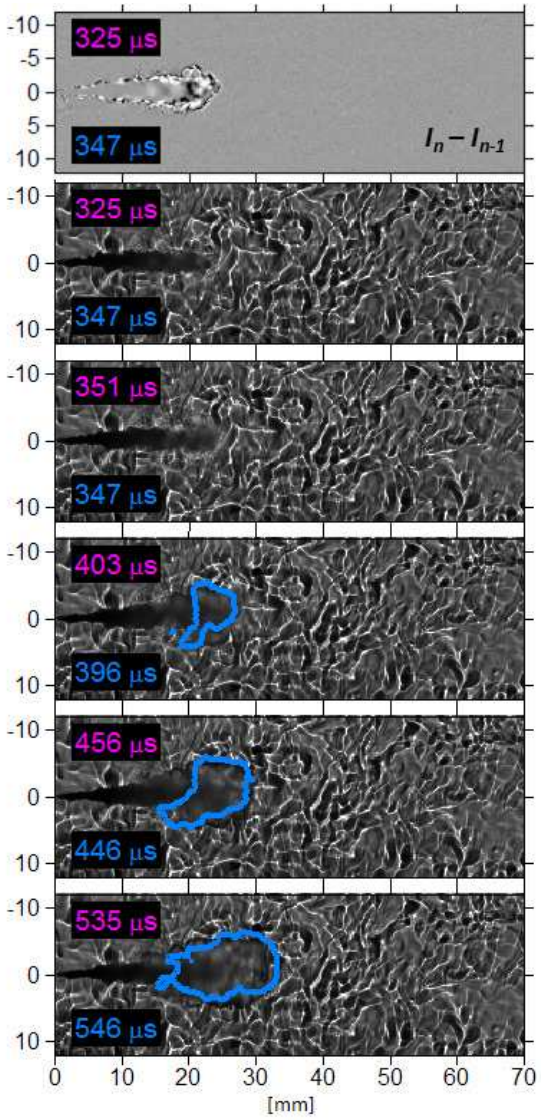

Figure 13: Schlieren images overlaid with broadband luminosity borders (blue) for the 900 K condition, test #3.

The 900 K condition in Figure 13 shows an ignition delay far advanced of the 750 K condition, with an associated shorter distance from the injector for the ignition site. Once again, the disappearance and reappearance schlieren phenomenon is observed in the downstream region of the jet during the time of ignition. The location of ignition occurs very near the tip of the jet.

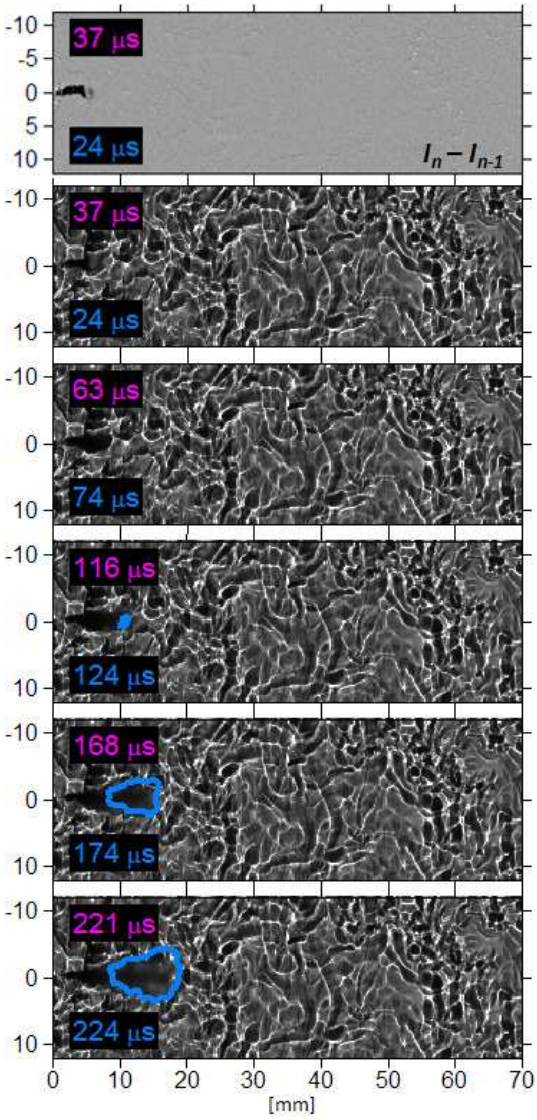

Figure 14: Schlieren images overlaid with broadband luminosity borders (blue) for the 1200 K condition, test #3.

The 1200 K condition shown in Figure 14 has a very short ignition delay and length. We do not observe the "disappearance" phenomenon near the tip of the jet prior to ignition, and the ignition location appears to be the very head of the impinging jet.

This method of combined schlieren and broadband chemiluminescence imaging proved useful in illustrating ignition progression. Schlieren imaging is effective in tracking gas-phase progression and ignition; however, exact borders of reacting zones are generally not easily recognizable. Broadband chemiluminescence serves as a compliment, providing clear high-temperature reaction borders. The uncertainty in temporal placement of optical data due to exposure duration is greater than 20 µs; more than that of pressure-based data. However, the high speed of light simplifies the interpretation of optical data, as measurement delay time is negligible. Future optical studies could also be performed using better temporal resolution, either with more capable equipment or reduced pixel resolution.

SPATIAL LOCATION OF IGNITION

A comparison between the pressure-triangulated ignition locations, which were shown in Table 6, and the optically established ignition locations shown in the schlieren and broadband luminescence imaging verifies that the pressure-based triangulation technique is accurate in detecting ignition location within about 3 mm. Other experiments not included in this paper generate similar conclusions.

The 750 K condition results are unique in that repeatability tests showed more variance in ignition location and timing. The third test for the 750 K condition had a shorter ignition length than the first two 750 K tests. The optical image sequence for that third test has already been shown in Figure 12, demonstrating that ignition occurs about 45 mm beyond the injector tip, or about 10 mm shy of the penetrating jet head. The triangulated distance is 43.5 mm for this condition, which is in good agreement. Referencing Table 6 indicates that the other two tests at the 750 K condition had ignition locations beyond 51 mm, much closer to the jet head. Figure 15 shows Test #1 for the 750 K condition at the start of high-temperature ignition. Notice that ignition occurs downstream of 50 mm, as triangulation predicted. Once again, this validates the pressure triangulation method on an injection-to-injection basis.

Variance of ignition location is more likely for low-temperature conditions where ignition delays are long and more sensitive to temperature. The ramifications of which may be high cycle-to-cycle variation if applied in real engines. Understanding the fluctuation in ignition location is a major step forward towards controlling and minimizing these fluctuations.

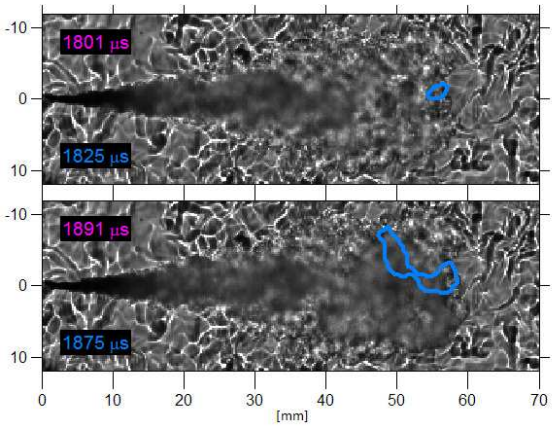

Figure 15: Schlieren images overlaid with broadband chemiluminescence border at the time of high-temperature ignition for Test#1 at 750 K.

DETECTION OF LOW-TEMPERATURE HEAT RELEASE

As shown in previous publications [7,20], the action of cool-flame combustion to break down the parent fuel and raise the temperature by mild heat release causes the refractive index of the cool-flame zone to be more similar to that of the ambient gases. This leads to a perceived “disappearance” of the region by schlieren imaging, as referred to above. In this section, we focus on these events by combining optical measurements with the improved understanding of the timing and position of the pressure-based measurements that multiple sensors affords.

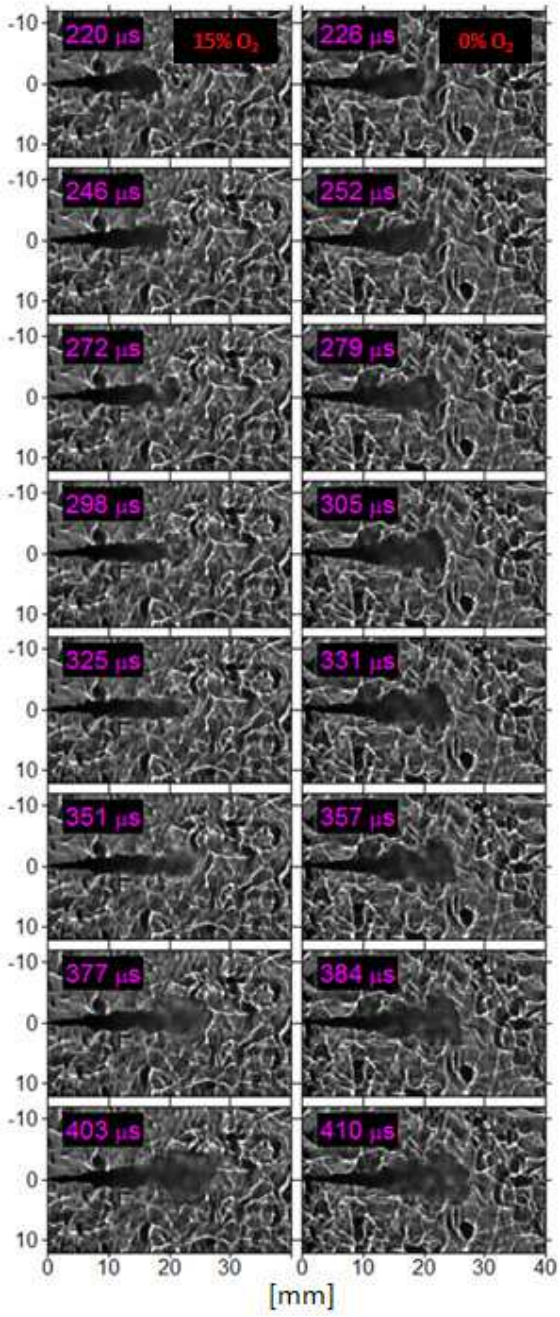

Figure 16: On the left is the schlieren imaging for the third test of the normal 900 K condition (15% O_2). On the right is the schlieren imaging for the same 900 K condition in the absence of oxygen (0% O_2, non-reacting).

Figure 16 shows the schlieren imaging for the third 900 K condition in contrast to its non-reacting equivalent. The camera setup was the same for both conditions. Ambient oxygen was removed for the non-reacting case, and all other properties, including the ambient gas thermal properties were held nearly that same. Therefore, any variance in the two conditions is expected to be a result of reactivity or heat release.

Notice that prior to the onset of high-temperature ignition (occurring strongly at 400 µs), regions of the jet become more transparent relative to the non-reacting jet, starting around the second frame (~245 µs) where the edges of the jet appear more eroded. These regions reappear at the time of high-temperature ignition and the schlieren effect produces a dark zone right at the edge of the jet. The effects are consistent with high-temperature gases and their accompanying intense refractive index gradients. Notice that neither the

disappearance, nor the darkening of the jet can be seen in the non-reactive case, indicating that both effects can be attributed to reaction.

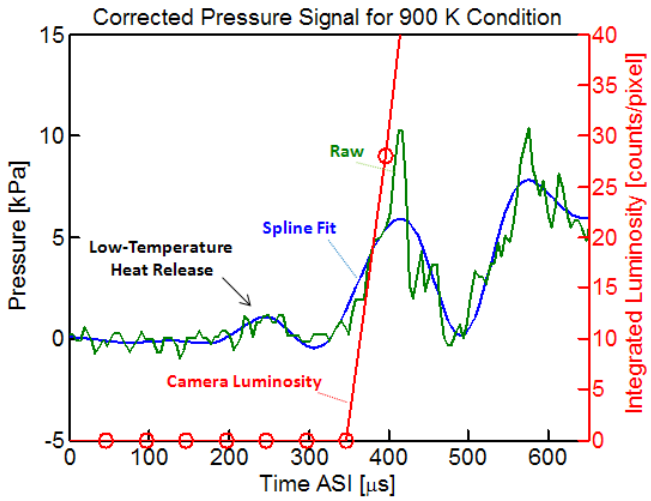

Figure 17: Pressure signal #2 for the 900 K condition focused around the time of ignition with the low-temperature combustion region highlighted. The time base for this figure has been properly corrected via the triangulation method.

Figure 17 shows the pressure signal from Transducer #2 during the ignition event for the 900 K condition, where the time base has been corrected (subtracted) for the 111 μs (Table 6) pressure wave delay, so that it is accurately placed in time relative to the start of injection, as is the optical data. The high-speed camera luminosity is also indicated on the figure, where it is shown as the integrated luminosity for all pixels. The onset of measureable luminosity agrees well with the pressure-indicated start of high-temperature heat release, a fact only realized because of the recognition of the pressure wave delay and its correction.

The improved pressure sensitivity of Transducer #2 (high charge-amp gain), along with the corrected time base, allows assessment of pressure changes caused by low-temperature combustion in addition to high-temperature combustion analysis. Figure 17 shows that low-temperature heat release causes a small pressure rise of only 1 kPa in magnitude beginning at about 220 μs and ending at around 300 μs. However, since the pressure time base is corrected mainly for the high-temperature ignition site, the time base to represent the cool flame needs a different correction. Table 6 shows that where heat-release events occur earlier, and closer to the injector, the time delay correction to Transducer #2 is less, for example, 90 μs at 1200 K conditions compared to 110 μs at 900 K conditions. Therefore, the cool flame pressure time base may need to be adjusted (increased) on the order of 20 μs. With this adjustment (*i.e.*, 220 μs to 240 μs), the schlieren imaging in Figure 16 is in good agreement with the pressure data. Clear indications of low-temperature combustion activity begin at 240 μs in the schlieren imaging, persisting for approximately 100 μs.

The pressure and schlieren data presented in previous sections for the 750 K condition also showed significant low-temperature activity prior to the onset of high-temperature combustion. This is further reinforcement that schlieren imaging can be a useful tool in detecting low-temperature combustion and ignition. This result is particularly useful because cool-flame chemiluminescence is weak and is difficult to detect with non-intensified imaging systems, as is shown in the luminosity signal given in Figure 17.

IMPLICATIONS OF TIME CORRECTION ON HEAT-RELEASE PHASING

Results demonstrated in Figure 17 for the 900 K condition emphasize the need to correct for the time delay of pressure to interpret the actual time of ignition. As discussed above, this time correction depends upon ignition location. By applying the time corrections listed in Table 6 to the pressure data given in Figures 8 and Figure 11, one can examine the corrected pressure timing with respect to chemiluminescence timing for the 1200 K and 700 K conditions. For example at 1200 K, the pressure peak for Transducer #2 shown in Figure 9 beginning at about 220 μs should be corrected by 90 μs, to indicate actual heat release begins at approximately 130 μs. This timing is in excellent agreement with the chemiluminescence and schlieren imaging given in Figure 14. Likewise for the 750 K condition, a correction of 142 μs brings the pressure data into closer alignment with the measured chemiluminescence. However, the time of first high-temperature combustion is not obvious based only on the pressure data, as there is a gradual rise in pressure during both cool-flame and the first high-temperature ignition kernels, as discussed above.

The three examples conditions given in this paper all required significant temporal correction of pressure data to indicate the actual ignition timing. As discussed in more detail in Ref. [6], the need for temporal correction of pressure data from engines should be considered, especially when this data is used primarily for model validation. The distance between the heat-release location and the pressure transducer may be smaller than that of this study, but the corrections may still be significant. Although ignition location will vary in an engine, just as in this study, a 20 mm distance between an ignition event and a cylinder-head-mounted pressure transducer would be common. This standoff may induce delays on the order of 30 μs, which would phase pressure by one-half crank angle degrees at engine speeds of 2500 RPM. Multiple ignition fronts produced by multi-hole injectors would also complicate the arrival time of multiple pressure waves to the transducer.

We acknowledge that the pressure correction routines implemented in this study have focused on the time of high-temperature ignition only. Before or after ignition, the reaction zone grows and or is more distributed, and multiple sources/locations of pressure rise arrive at the same time at the transducer. For a developed flame, various options for pressure data correction exist. Defining the spatial center of a reactive zone could be used in a dynamic pressure correction algorithm. For example, the reaction zone tends to propagate from the ignition site to the head of the penetrating jet. Correlations for the rate of penetration of the jet could be implemented to perform different corrections with respect to time after the start of injection and ambient conditions, as discussed in Ref. [28].

SUMMARY/CONCLUSIONS

Diesel ignition has been studied in a constant-volume combustion vessel under three ambient temperature conditions, 750 K, 900 K and 1200 K. A pressure-based location triangulation approach was implemented using multiple pressure transducers to determine the ignition events temporal and spatial origins. This location and timing was then compared to high-speed schlieren and broadband chemiluminescence imaging to confirm the validity of the technique. The following are significant conclusions of the study:

1. The pressure triangulation technique determined diesel ignition location to accuracies within approximately 3 mm, over the range of conditions where the ignition location varied by more than 40 mm.

2. By identifying the ignition site, speed-of-sound time corrections can be applied to the measured pressure to understand the correct timing of ignition. Comparison with high-speed chemiluminescence imaging shows that the time adjustment of pressure correlates with the actual ignition timing.

3. The use of multiple transducers permits gain optimization for pressure rise of the spray, rather than the combustion chamber, thereby providing significantly improved pressure-rise measurement and derived heat-release rate for the diesel spray.

4. With improved pressure sensitivity and timing, pressure activity based on first-stage, cool-flame activity can be compared to schlieren imaging. The apparent “disappearance” of the schlieren effect correlates with the onset of low-temperature heat-release in the pressure-based data. This schlieren effect is consistent with the hypothesis that small amounts of heat-release decompose the fuel and raise the local temperature such that the cool-flame spray regions match the refractive index of the ambient.

REFERENCES

1. Gopalakrishnan, V., Abraham, J., “An Investigation of Ignition and Heat Release Characteristics in a Diesel Engine Using an Interactive Flamelet Model,” SAE Paper 2003-01-1062
2. Liang, L., Chitralkumar, V.N., Puduppakkam, K., Wang, C., Modak, A., Meeks,E., Ge, H.W., Reitz, R., Rutland,C., “Efficient Simulation of Diesel Engine Combustion Using Realistic Chemical Kinetics in CFD,” SAE Paper 2010-01-0178
3. Singh, S., Reitz, R.D., Musculus, M.P.B., “Comparison of the Characteristic Time (CTC), Representative Interactive Flamelet (RIF), and Direct Integration with Detailed Chemistry Combustion Models against Optical Diagnostic Data for Multi-Mode Combustion in a Heavy-Duty DI Diesel Engine,” SAE Paper 2006-01-005
4. Lucchini, T., D’Errico, G., Ettorre, D., Brusiani, F., Bianchi, G.M., Montanaro, A., Allocca, L., “Experimental and Numerical Investigation of High-Pressure Diesel Sprays with Multiple Injections at Engine Conditions,” SAE Paper 2010-01-0179
5. Farrell, J.T., Cernansky, N.P., Dryer, F.L., Friend, D.G., Hergart, C.A., Law, C.K., McDavid, R.M., Mueller, C.J., Patel, A.K., Pitsch, H., “Development of an Experimental Database and Kinetic Models for Surrogate Diesel Fuels,” SAE Paper 2007-01-0201
6. Higgins, B., Siebers, D., “Diesel-Spray Ignition and Premixed-Burn Behavior,” SAE Paper 2000-01-0940
7. Pickett, L.M., Kook, S., Williams, T.C., “Visualization of Diesel Spray Penetration, Cool-Flame, Ignition, High-Temperature Combustion, and Soot Formation Using High-Speed Imaging,” SAE Paper 2009-01-0658

8. Pickett, L.M., Siebers, D.L., Idicheria, C.A., “Relationship Between Ignition Processes and Lift-Off Length of Diesel Fuel Jets,” SAE Paper 2005-01-3843
9. Polonowski, C., Mueller, C., Gehrke, C., Bazyn, T., Martin, G., and Lillo, P., "An Experimental Investigation of Low-Soot and Soot-Free Combustion Strategies in a Heavy-Duty, Single-Cylinder, Direct-Injection, Optical Diesel Engine," JSAE 20119091 / SAE 2011-01-1812, 2011
10. Dec, J.E., Espey, C., “Chemiluminescence Imaging of Autoignition in a DI Diesel Engine,” SAE Paper 982685
11. Bobba, M., Genzale, C., Musculus, M., “Effect of Ignition Delay on In-Cylinder Soot Characteristics of a Heavy Duty Diesel Engine Operating at Low Temperature Conditions,” SAE Paper 2009-01-0946
12. Jansons, M., Brar, A., Estefanous, F., Florea, R., Taraza, D., Henein, N., Bryzik, W., “Experimental Investigation of Single and Two-Stage Ignition in a Diesel Engine,” SAE Paper 2008-01-1071
13. Davis, R.S., Patterson, G.J., “Cylinder Pressure Data Quality Checks and Procedures to Maximize Data Accuracy,” SAE Paper 2006-01-1346
14. Higuma, A., Suzuki, T., Yoshida, M., Oguri, Y., Minoyama, T., “Improvement of Error in Piezoelectric Pressure Transducer,” SAE Paper 1999-01-0207
15. Randolph, A.L., “Methods of processing cylinder-pressure transducer signals to maximize data accuracy,” SAE Paper 900170
16. König, G., Maly, R., Bradley, D., Lau, A.K.C., and Sheppard, C.G.W., "Role of Exothermic Centers on Knock Initiation and Knock Damage," SAE Paper 902136, 1990
17. Liiva, P.M., Valentine, J.N., Cobb, J.M., and Acker, W.P., "Use of Multiple Pressure Transducers to Find In-Cylinder Knock Location," SAE Paper 922368, 1992
18. Vressner, A., Lundin, A., Christensen, M., Tunestål, P., and Johansson, B., "Pressure Oscillations During Rapid HCCI Combustion," SAE Paper 2003-01-3217, 2003
19. Spicher, U., Kröger, H., and Ganser, J., "Detection of Knocking Combustion Using Simultaneously High-Speed Schlieren Cinematography and Multi Optical Fiber Technique," SAE Paper 912312, 1991
20. Pickett, L.M., Genzale, C., Bruneaux, G., Malbeck, L.M., Hermant, L., Christiansen, C., Schramm, J., “Comparison of diesel spray combustion in different high-temperature, high pressure facilities,” SAE Paper 2010-01-2106
21. Higgins, B., Siebers, D., “Measurement of the Flame Lift-Off Location on DI Diesel Sprays Using OH Chemiluminescence,” SAE Paper 2001-01-0918
22. Pickett, L.M., Manin, J., Genzale, C.L., Siebers, D.L., Musculus, M.P.B., and Idicheria, C.A., "Relationship between diesel fuel spray vapor penetration/dispersion and local fuel mixture fraction," SAE Int. J. Engines 4:764-799, doi:10.4271/2011-01-0686
23. Pickett, L.M., Siebers, D.L., “Non-sooting, low flame temperature mixing-controlled DI diesel combustion,” SAE Paper 2004-01-1399
24. Pickett, L.M., Idicheria, C.A., “Formaldehyde Visualization Near Lift-off Location in a Diesel Jet,” SAE Paper 2006-01-3434
25. Settles, G.S., Schlieren and Shadowgraph Techniques, Springer-Verlag, 2001.
26. Mueller, C.J., Martin, G.C., “Effects of Oxygenated Compounds on Combustion and Soot Evolution in a DI Diesel Engine: Broadband Natural Luminosity Imaging,” SAE Paper 2002-01-1631
27. Musculus, M., “Measurements of the Influence of Soot Radiation on In-Cylinder Temperatures and Exhaust NOx in a Heavy-Duty DI Diesel Engine,” SAE Paper 2005-01-0925
28. Engine Combustion Network data archive. http://www.sandia.gov/ecn/

CONTACT INFORMATION

Peter M. Lillo (plillo@umich.edu)

ACKNOWLEDGMENTS

Support for this research was provided by the U.S. Department of Energy, Office of Vehicle Technologies. The Swedish Foundation for Strategic Research supported Helena Persson’s visiting research financially. The research was performed at the Combustion Research Facility, Sandia National Laboratories, Livermore, California. Sandia is a multiprogram laboratory operated by Sandia Corporation, a Lockheed Martin Company, for the United States Department of Energy’s National Nuclear Security Administration under contract DE-AC04-94AL85000.